RADIO SCIENCE, VOL. 43, RS5008, doi:10.1029/2007RS003817, 2008

Estimate of higher order ionospheric errors in GNSS positioning

M. Mainul Hoque[1,2] and N. Jakowski[1]

Received 17 December 2007; revised 15 May 2008; accepted 9 June 2008; published 9 October 2008.

[1] Precise navigation and positioning using GPS/GLONASS/Galileo require the ionospheric propagation errors to be accurately determined and corrected for. Current dual-frequency method of ionospheric correction ignores higher order ionospheric errors such as the second and third order ionospheric terms in the refractive index formula and errors due to bending of the signal. The total electron content (TEC) is assumed to be same at two GPS frequencies. All these assumptions lead to erroneous estimations and corrections of the ionospheric errors. In this paper a rigorous treatment of these problems is presented. Different approximation formulas have been proposed to correct errors due to excess path length in addition to the free space path length, TEC difference at two GNSS frequencies, and third-order ionospheric term. The GPS dual-frequency residual range errors can be corrected within millimeter level accuracy using the proposed correction formulas.

Citation: Hoque, M. M., and N. Jakowski (2008), Estimate of higher order ionospheric errors in GNSS positioning, *Radio Sci.*, *43*, RS5008, doi:10.1029/2007RS003817.

1. Introduction

[2] The ionosphere is a significant error source of the GNSS error budget. Ionosphere-induced range errors vary from a few meters to tens of meters at the zenith [*Klobuchar*, 1996]. Since the ionosphere is a dispersive medium, the most part of the ionospheric delay can be eliminated through linear combinations of dual-frequency observables; therefore, only the higher order ionospheric errors will remain in the range estimation. However these errors can reach several tens of centimeters at low elevation angles and during extreme space weather conditions (i.e., ionospheric storms), which represent large errors in geodetic measurements [*Klobuchar*, 1996]. Satellite positions can also be improved to the centimeter level when higher order ionospheric corrections are applied [*Fritsche et al.*, 2005].

[3] Early work is done by *Brunner and Gu* [1991] in developing correction models for higher order ionospheric errors, especially to correct the second-order term and raypath bending error. Their approach requires the knowledge of the actual ionosphere and the average value of the longitudinal component of the Earth's magnetic field along raypaths. In practical cases, these parameters are not easy to estimate accurately.

[4] Later *Bassiri and Hajj* [1993] have done similar work assuming an Earth-centered tilted dipole approximation for the geomagnetic field. They consider the ionosphere as a single (thin) layer at a certain altitude (300 km) and compute the magnetic field vector at the ionospheric pierce point (IPP). However investigation by *Hawarey et al.* [2005] for Very Long Baseline Interferometry (VLBI) shows that further improvements for the second-order ionospheric term can be achieved using a more realistic magnetic field model such as the International Geomagnetic Reference Field (IGRF) instead of a dipole model.

[5] *Strangeways and Ioannides* [2002] presented a method for the range correction to less than 1 cm accuracy by employing three factors: one representing the ratio of the slant TECs experienced by the two frequencies and the other two representing the ratio of their geometric path lengths with respect to the true range. However, these parameters are not easy to estimate accurately in practical cases.

[6] In our previous work [*Hoque and Jakowski*, 2006, 2007], we proposed models for the second-order ionospheric error correction as a function of geographic latitude and longitude and geometrical parameters such as elevation and azimuth angles for GNSS users in

[1]German Aerospace Center (DLR), Institute of Communications and Navigation, Neustrelitz, Germany.
[2]International Postgraduate Programme Multi Sensorics, Center for Sensorsystems, University of Siegen, Siegen, Germany.

0048-6604/08/2007RS003817$11.00

Germany and Europe (latitude range 30–65°N, longitude range 15°W–45°E).

[7] In the present work, we have derived approximation formulas to estimate and correct dual-frequency range errors due to excess path length of the signal in addition to the free space path length, TEC difference at two GNSS frequencies, and third-order ionospheric term.

2. Higher Order Ionospheric Errors

[8] Assuming a right-hand circularly polarized signal, the GNSS code (Ψ) and phase (Φ) pseudo-range equations in terms of higher order ionospheric errors can be written as [*Bassiri and Hajj*, 1993; *Hoque and Jakowski*, 2006]

$$\Psi_i = \rho + \frac{p_i}{f_i^2} + \frac{q}{f_i^3} + \frac{t}{f_i^4} + d_i^{b(length)} \tag{1}$$

$$\Phi_i = \rho - \frac{p_i}{f_i^2} - \frac{q}{2f_i^3} - \frac{t}{3f_i^4} + d_i^{b(length)} \tag{2}$$

respectively, in which

$$p_i = 40.3 \int n_e ds = 40.3 \times TEC_i = 40.3 \times (TEC_{LoS} + \Delta TEC_i) \tag{3}$$

$$q = 2.2566 \times 10^{12} \int n_e B \cos\Theta \cdot ds \tag{4}$$

$$t = 2437 \int n_e^2 ds + 4.74 \times 10^{22} \int n_e B^2 \left(1 + \cos^2\Theta\right) ds \tag{5}$$

where the index i = 1, 2,..., refers to the GNSS carrier frequencies (in case of GPS, f_1 = 1575.42 MHz and f_2 = 1227.6 MHz), ρ is the geometric distance between the transmitter and the receiver also known as the true range, n_e is the electron concentration, ds is the raypath element, Θ is the angle between the ray direction and the magnetic field vector $\boldsymbol{B}$, and B is the magnitude of $\boldsymbol{B}$. The integral $\int n_e ds$ along the raypath is the total electron content (TEC) often measured in TEC units (1 TECU = 10^{16} electrons/m^2). The additional term $d_i^{b(length)}$ at the right-hand side of equations (1) and (2) corresponds to the excess path length of the signal in addition to the free space path length.

[9] Due to the dispersive nature of the ionosphere, GNSS signals travel along different raypaths through the ionosphere and TEC along f_1 path will be different from that along f_2 path and from that along the straight line of sight (LoS). Considering this, TEC in equation (3) is separated into $\mathrm{TEC_{LoS}}$, which is along the straight LoS, and $\Delta\mathrm{TEC}_i$, which is the difference between TEC along the LoS and the raypath.

[10] The first-order ($1/f^2$) ionospheric error can be eliminated by constructing a linear combination of dual-frequency observables. In case of GPS, this approach is known as ionosphere-free linear L3 combination. However the second ($1/f^3$)- and third-order ($1/f^4$) ionospheric terms, the error due to TEC difference along f_1 and f_2 paths, and the excess path length $d_i^{b(length)}$ will not be canceled out in this approach. Therefore, dual-frequency (f_1 and f_2) code and phase combinations can be written as (using equations (1) and (2))

$$\frac{f_1^2}{f_1^2 - f_2^2}\Psi_1 - \frac{f_2^2}{f_1^2 - f_2^2}\Psi_2 = \rho \underbrace{-\Delta s_{b(TEC)} - 2\Delta s_2 - 3\Delta s_3 - \Delta s_{b(length)}}_{(RRE)_{gr}} \tag{6}$$

$$\frac{f_1^2}{f_1^2 - f_2^2}\Phi_1 - \frac{f_2^2}{f_1^2 - f_2^2}\Phi_2 = \rho \underbrace{+\Delta s_{b(TEC)} + \Delta s_2 + \Delta s_3 - \Delta s_{b(length)}}_{RRE} \tag{7}$$

In which

$$\Delta s_{b(TEC)} = \frac{40.3 \times (TEC_2 - TEC_1)}{\left(f_1^2 - f_2^2\right)} = \frac{40.3 \times (\Delta TEC_2 - \Delta TEC_1)}{\left(f_1^2 - f_2^2\right)} \tag{8}$$

$$\Delta s_2 = \frac{q}{2f_1 f_2 (f_1 + f_2)} \tag{9}$$

$$\Delta s_3 = \frac{t}{3f_1^2 f_2^2} \tag{10}$$

$$\Delta s_{b(length)} = \frac{d_2^{b(length)} f_2^2 - d_1^{b(length)} f_1^2}{\left(f_1^2 - f_2^2\right)} \tag{11}$$

where $\mathrm{TEC_1}$ and $\mathrm{TEC_2}$ are the total electron content along f_1 and f_2 paths, and these TEC values are larger than $\mathrm{TEC_{LoS}}$ by amounts of $\Delta\mathrm{TEC_1}$ and $\Delta\mathrm{TEC_2}$, respectively, the terms Δs_2 and Δs_3 are referred to as the dual-frequency second and third-order residual error, respectively, $\Delta s_{b(length)}$ and $\Delta s_{b(TEC)}$ are referred to as the dual-frequency residual errors due to excess path length and TEC difference (along f_1 and f_2 paths), respectively. Adding all these terms, $(\mathrm{RRE})_{\mathrm{gr}}$ and RRE

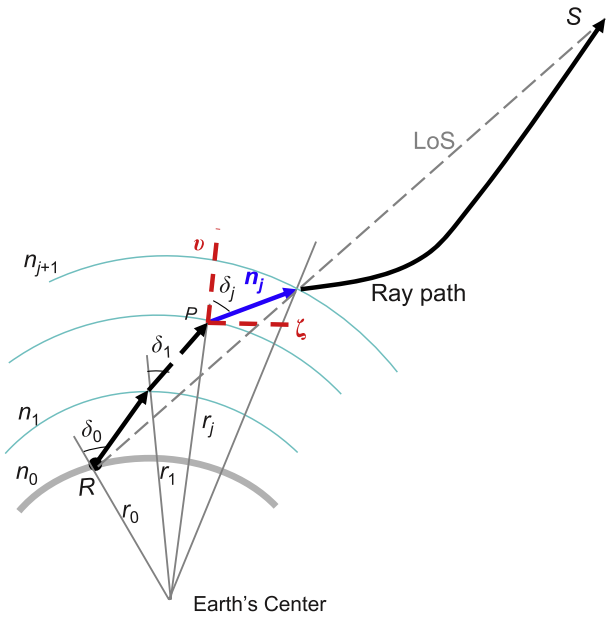

Figure 1. Ray tracing in the non homogeneous anisotropic ionosphere.

are obtained, which correspond to the dual-frequency total residual range error for code and phase combinations, respectively (see equations (6) and (7)). The only way to investigate all these errors is to trace rays through the ionosphere.

3. Ray Tracing Through the Ionosphere

[11] A two-dimensional ray tracing program is developed to trace rays through a user specified model of the ionosphere. We assume models for the electron density n_e and the Earth's magnetic field $\boldsymbol{B}$. The electron density at an ionospheric height h can be well described by a Chapman layer and written as [*Rishbeth and Garriott*, 1969]

$$n_e(h) = N_0 \exp(0.5(1 - z - \sec\ \chi \cdot \exp(-z))) \quad (12)$$

where $z = (h - h_0)/H$, H is the atmospheric scale height, χ is the sun's zenith angle, and N_0 is the peak electron density at the altitude h_0 at zenith ($\chi = 0$). It can be seen that $n_e(h)$ has a maximum value $N_m = N_0\sqrt{\cos\ \chi}$ at the altitude $h_m = h_0 + H \ln(\sec\ \chi)$ [*Budden*, 1985]. In our previous paper [*Hoque and Jakowski*, 2007], n_e profiles are modeled as the sum of three Chapman layers describing electron densities of the ionospheric F_2, F_1, and E layers and a superposed exponential decay function for the plasmasphere. The layer parameters are chosen from wide ranges (for F_2 layer h_mF_2 range 250–400 km, HF_2 range 60–80 km; for F_1 layer h_mF_1 range 180–220 km, HF_1 range 40–60 km, and for E layer h_mE range 100–120 km, HE range 5–15 km). The same ionosphere modeling is used here. For the Earth's magnetic field, the IGRF model [*Mandea and Macmillan*, 2000] is used to calculate $\boldsymbol{B}$ vectors along raypaths.

[12] However the limitations of modeling the ionosphere with Chapman layers may limit the accuracies obtained in the higher order ionospheric term estimation. Therefore, a large number (about 20,000) of n_e profiles reconstructed from GPS radio occultation measurements onboard the CHAMP satellite (available at http://w3swaci.dlr.de/) are used to validate the results obtained by Chapman profiles. The radio occultation measurements onboard low Earth orbiting (LEO) satellites can provide vertical electron density profiles of the ionosphere from satellite orbit heights down to the bottomside. The retrieval algorithm uses an adaptive model for estimating the topside ionosphere and plasmasphere above the CHAMP orbit height [*Jakowski et al.*, 2002; *Jakowski*, 2005].

[13] Now the refraction of the ray can be calculated in realistic ways assuming the ionosphere to be composed of a large number of thin spherical shells, in each of which the medium is homogeneous (see Figure 1). The refraction angle at an arbitrary jth layer can be determined by Bouguer's law (Snell's law in spherical surface) of refraction as [*Croft and Hoogasian*, 1968]

$$\delta_j = \arcsin\left(\frac{r_0}{r_j n_j}\sin\delta_0\right) \quad (13)$$

where δ_0 is the zenith angle ($\pi/2-$ elevation) at the Earth's surface where the refractive index $n_0 = 1$, δ_j is the refraction angle at the jth layer (where $n_j \neq 1$), and r_0 and r_j are the radial distances (from the Earth's center) at the surface and at the jth layer, respectively. In general, for a radio wave of frequency f, the refractive index n is given by the Appleton–Hartree formula [*Budden*, 1985] as

$$n^2 = 1 - \frac{2X(1-X)}{2(1-X) - Y^2\sin^2\Theta \pm \left[Y^4\sin^4\Theta + 4(1-X)^2Y^2\cos^2\Theta\right]^{\frac{1}{2}}} \quad (14)$$

in which $X = n_e e^2/(4\pi^2\varepsilon_0 m f^2)$, $Y = eB/(2\pi m f)$ where e and m are the electron charge and mass, respectively, and ε_0 is the permittivity of the free space.

[14] Regardless of the vertical distribution of the refractive index, the angle of refraction is given by equation (13). However, when the medium is anisotropic,

Bouguer's law cannot readily be used. In this case, the unknown angle δ_j could be found from equation (13) if n_j were known, but n_j depends on the angle Θ between the wave normal and the geomagnetic vector $\boldsymbol{B}$ (see equation (14)), and this angle in turn depends on δ_j.

[15] Since the anisotropic plasma is doubly refracting (indicated by the ± sign in refractive index equation (14)) there are actually two waves. The wave with the upper (+) sign is usually called the ordinary wave, whereas the lower (−) sign is related to the extraordinary wave. The ordinary mode is left-hand circularly polarized, while the extra-ordinary mode is right-hand circularly polarized [*Hartmann and Leitinger*, 1984]. However, since GPS signals are transmitted in the right-hand polarization [*Parkinson and Gilbert*, 1983], only the results of extraordinary mode are considered here.

[16] To solve the refractive index equation in an anisotropic plasma, a two-dimensional Cartesian coordinate system (ζ, υ) with ζ horizontal and υ vertically upward (i.e., along the radius) axes is considered here. The introduction of such a coordinate system to solve this problem is already described by *Budden* [1985] for the plane ionosphere. To take into account the effect of the Earth's curvature on ray propagation, this concept is used here for the spherically layered ionosphere.

[17] In the jth stratum, the wave normal makes an angle δ_j with the υ axis (see Figure 1). The refractive index is considered as a vector $\boldsymbol{n}_j$ with magnitude n_j and in the direction of the wave normal, and $\boldsymbol{B}$ field components are computed along ζ and υ axes. Taking dot products of $\boldsymbol{n}_j$ and $\boldsymbol{B}$, the angle Θ between them can be determined. In this approach, two unknowns (n_j and Θ) in equation (14) can be replaced by one unknown, which results in a quartic equation known as Booker quartic [*Booker*, 1949]. For details of this approach, we refer to *Budden*, 1985.

[18] Ray tracing determines the raypath between a known transmitter and a receiver for a given frequency in a user specified ionosphere model. In general, ray tracing starts from specified angles of elevation and azimuth, so the ray may miss the target. This problem is known as homing-in problem. To solve this problem Nelder–Mead [*Nelder and Mead*, 1965] simplex algorithm is implemented in the ray tracing program. It has been found that the simplex method using Nelder–Mead algorithm works very reliably when solving the raypath homing-in problem [*Strangeways*, 2000; *Strangeways and Ioannides*, 2002].

[19] The ray tracing program is checked by comparing its results with the results given by *Brunner and Gu* [1991]. Brunner and Gu used a three-dimensional ray tracing technique based on differential equations [*Haselgrove*, 1963]. It has been found that excess path lengths estimated by the two methods do not differ more than one millimeter even at low elevation (e.g., 7.5°) and high vertical TEC values (455 TECU) at GPS frequencies. The ray tracing program is used to develop empirical formulas and also to verify analytical solutions of different higher order ionospheric corrections proposed in this paper.

4. Second Order Ionospheric Term

[20] The effect of the Earth's magnetic field on radio wave propagation, which is known as the magneto-ionic effect or second-order ionospheric effect, is investigated in our previous work [*Hoque and Jakowski*, 2006, 2007]. Empirical formulas are developed to estimate and correct the second-order ionospheric effect on GNSS users in Germany and Europe.

[21] Since tracing of the magneto-ionic interaction (between the ionosphere and the geomagnetic field) along raypaths is very cumbersome, a common practice is to assume the ionosphere as a single (thin) layer at a certain altitude and compute the magnetic field vector $\boldsymbol{B}$ at the IPP. Thus, the second-order error coefficient q (see equation (4)) can be written as

$$q \approx 2.2566 \times 10^{12} \cdot B \cos\Theta \cdot TEC \qquad (15)$$

where B and Θ will be estimated at the IPP. *Bassiri and Hajj* [1993] were the first to propose such a single layer thin ionosphere assumption for the second-order ionospheric correction; they choose a representative global average peak height as 300 km. Later *Kedar et al.* [2003] assumes the ionosphere as a single layer at a 400-km altitude and estimates the effect of the second-order GPS ionospheric correction on receiver positions. Recently, *Hernandez-Pajares et al.* [2007] considers the ionosphere as a single layer at a 450-km altitude to estimate impacts of second-order ionospheric term on geodetic estimates.

[22] However such assumption for the B cos Θ computation introduces errors in the second-order ionospheric term estimations. In the following, these errors will be investigated by estimating the GPS dual-frequency (L1–L2) residual error Δs_2 by two ways: (1) computing B cos Θ along raypaths and (2) computing B cos Θ only at the IPP (400 km). Then, the differences between the two estimations (Δs_2 by first method $-\Delta s_2$ by second method) are derived at elevation 90° and 5° for azimuth 0° and 180° over the globe. These values are plotted in Figure 2. The ionosphere is modeled by a Chapman layer with a maximum ionization of about 4.96×10^{12} electrons/m^3 at an altitude of 400 km and TEC in vertical direction (TEC_V) is estimated to be about 143 TECU.

[23] We see that at 180° azimuth (see Figure 2(a)), Δs_2 is positive for the northern hemisphere and also for a large part of the southern hemisphere (at low and mid

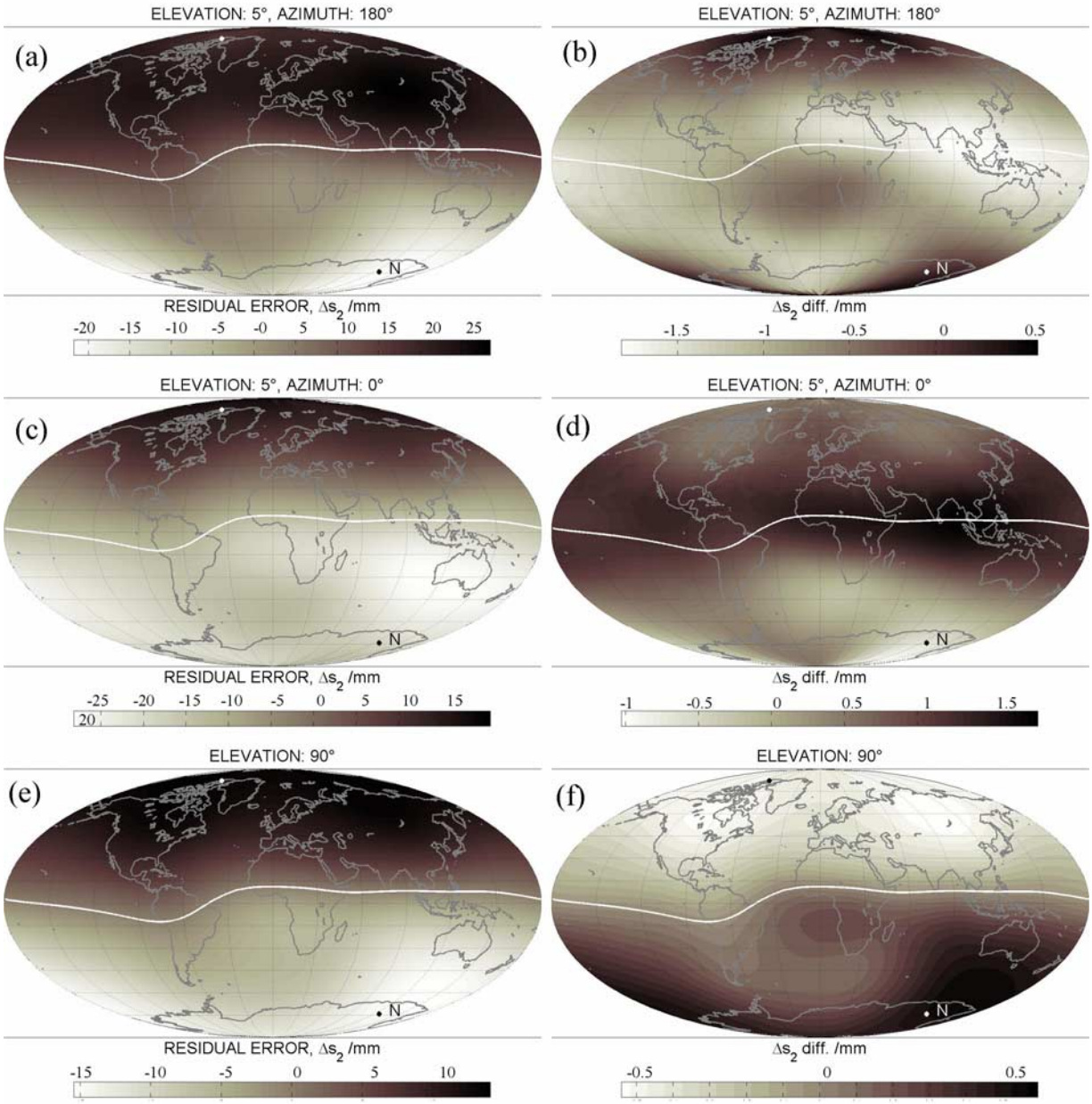

Figure 2. Global Δs_2 variations computed by the first method are plotted for: (a) elevation, $\beta = 5°$ and azimuth, $\alpha = 180°$, (c) $\beta = 5°$ and $\alpha = 0°$ and (e) $\beta = 90°$. The corresponding Δs_2 differences between the two methods are plotted in (b), (d) and (f) panels, respectively.

latitudes) and negative for the rest of the globe. The maximum Δs_2 is estimated to be about 28.8 mm in the northern hemisphere at about 45°N latitude and 100°E longitude.

[24] At 0° azimuth (see Figure 2(c)), Δs_2 is negative for the southern hemisphere and also for a large part of the northern hemisphere (at low latitudes) and positive for the rest of the globe. The maximum (absolute value) Δs_2 is estimated to be about −28.5 mm in the southern hemisphere at about (35°S, 120°E).

[25] The Δs_2 difference plots in Figure 2(b, d) show that large differences are occurred along the geomagnetic

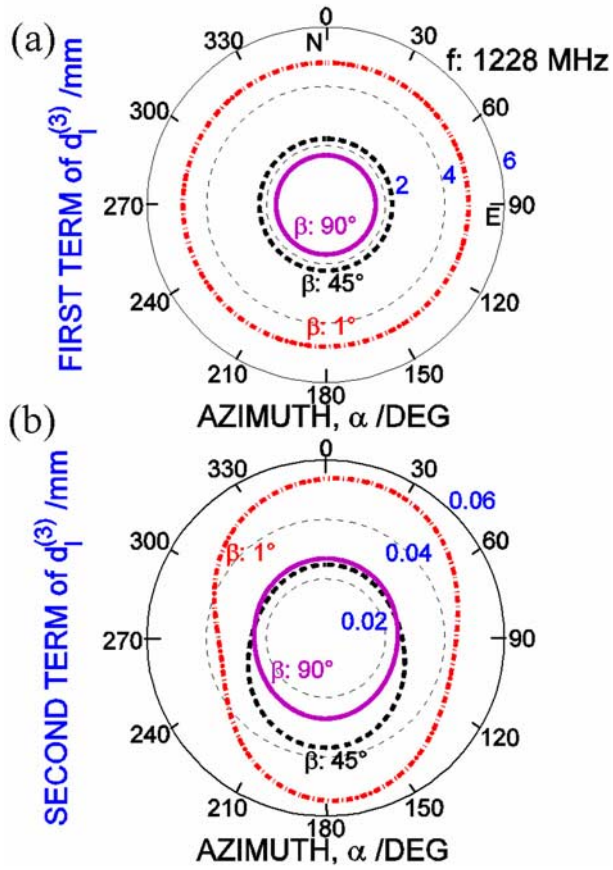

Figure 3. Variations of the (a) first term and (b) second term of $d_I^{(3)}$ (equation (16)) with azimuth at L2 frequency and TEC_V = 143 TECU.

equator. In case of 180° azimuth, the maximum (absolute value) difference is found to be about −1.9 mm at about (10°N, 100°E) whereas in case of 0° azimuth, the maximum difference is found to be about 1.9 mm at about (5°N, 95°E).

[26] Figure 2(e) shows that at zenith propagation (90° elevation), Δs_2 values are directly proportional to the vertically downward component of the geomagnetic field, that is, these values are large at poles and vanish at equator [also see *Hoque and Jakowski*, 2006]. The difference plot (see Figure 2(f)) shows that Δs_2 values are overestimated (i.e., negative) in the northern hemisphere and underestimated in the southern hemisphere by the second method. The large differences are observed in the poles and not in the equatorial regions. The percentage error (Δs_2 difference/Δs_2 by first method) × 100% is found to be about 10% at elevation 5° and about 5% at zenith on an average. Therefore, computing B cos Θ only at the IPP does not give the most accurate Δs_2 estimation. Considering this, B cos Θ is computed along raypaths for Δs_2 estimation in later sections.

5. Third-Order Ionospheric Term

[27] To correct the third-order ionospheric term, a correction formula based on analytical integration of Chapman function will be derived here. The third-order ionospheric phase error term can be separated from other higher order terms as (see equation (2))

$$d_I^{(3)} = \frac{t}{3f_i^4} = \frac{812.3}{f_i^4}\int n_e^2 ds + \frac{1.58\times 10^{22}}{f_i^4}\int n_e B^2\left(1+\cos^2\Theta\right)ds \qquad (16)$$

[28] The first and second terms in the right-hand side of equation (16) are estimated separately by the ray tracing program for GPS L2 frequency at a receiver location with geographic latitude 48°N and longitude 15°E. Their values are plotted in Figure 3. In these polar plots, the third-order phase error components are plotted as radial distances from the center of the polar plot while (receiver-to-satellite) azimuth angle is varied from 0° to 360° for three elevations β = 1°, 45°, and 90°.

[29] Since the horizontal gradient of n_e is ignored in simulation process, the first term of $d_I^{(3)}$ is independent of azimuth (see Figure 3(a)), but the second term depends on azimuth (due to dependency on B) and has the maximum magnitude in the North-South direction. The second term of $d_I^{(3)}$ is found to be less than the first term by about 1–2 orders of magnitude. Therefore, the second term will not be considered in determining correction formula for the third-order term. Thus, equation (16) can be simplified as

$$d_I^{(3)} \approx \frac{812.3}{f_i^4}\int n_e^2 ds \qquad (17)$$

The approximate solution of equation (17) for a Chapman profile can be written at χ = 0 as (see Appendix B)

$$d_I^{(3)} \approx \frac{812.3}{f_i^4}\frac{H(h_m+R_E)N_m^2\exp(1)}{\sqrt{(h_m+R_E)^2-(R_h+R_E)^2\cos^2\beta}} \qquad (18)$$

where N_m is the maximum ionization at altitude h_m, R_h is the receiver altitude, R_E is the (mean) radius of the Earth, and β is the elevation angle at R_h.

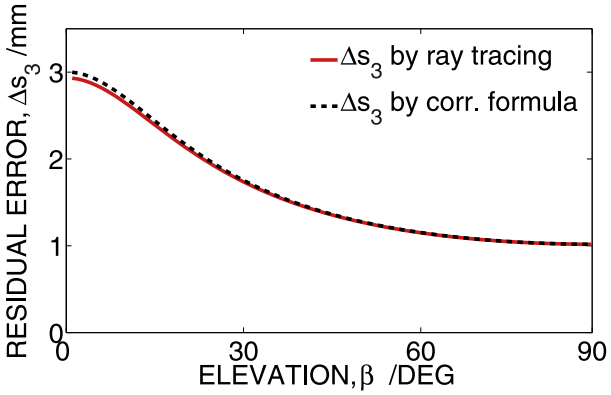

Figure 4. Variations of Δs_3 estimated by the correction formula (equation (21)) (dotted curve) and by the ray tracing program (solid line) at TEC_V = 143 TECU.

[30] Again, the analytical solution of TEC expression for a Chapman layer can be written at $\chi = 0$ as (see Appendix A)

$$TEC \approx \frac{H(h_m + R_E)N_m\sqrt{2\pi\exp(1)}}{\sqrt{(h_m + R_E)^2 - (R_h + R_E)^2\cos^2\beta}} \quad (19)$$

Now, equation (18) can be written as

$$d_I^{(3)} \approx \frac{812.3}{f_i^4}\frac{N_m\sqrt{\exp(1)}}{\sqrt{2\pi}}TEC \approx \frac{812.3}{f_i^4} \times 0.6577N_mTEC \quad (20)$$

Comparing equations (17) and (20), the integral $\int n_e^2 ds$ can be written as $\int n_e^2 ds \approx 0.6577N_m$TEC, this expression is very useful to determine the so-called shape parameter η ($=\int n_e^2 ds/(N_m \cdot TEC)$ [*Hartmann and Leitinger*, 1984; *Leitinger and Putz*, 1988; *Brunner and Gu*, 1991]) of the ionosphere profile. *Brunner and Gu* [1991] found that η hardly varies with elevation and N_m, and they estimated η to be 0.6635 at elevation 7.5° and 0.6498 at 90°. The analytical solution of η = 0.6577 for a Chapman layer agrees with their results.

[31] Now using the expression $\int n_e^2 ds \approx 0.6577N_mTEC$, the dual-frequency third-order residual error (equation (10)) can be simplified as

$$\Delta s_3 = \frac{812.3}{f_1^2 f_2^2} \times 0.6577N_mTEC = \frac{534.25}{f_1^2 f_2^2}N_mTEC \quad (21)$$

[32] To check the accuracy of the correction formula (equation (21)), the residual error Δs_3 is estimated by the ray tracing program and by the correction formula. These values are plotted with elevation angle in Figure 4.

[33] Figure 4 shows that the differences between Δs_3 estimated by the two methods are in the submillimeter level and can be ignored. If the ionosphere is modeled by adding a number of Chapman layers, for each layer the third-order phase error can be determined by the approximation formula and added together for the resultant error.

[34] As already mentioned, the limitation of modeling the ionosphere with Chapman layers limits the accuracies obtained in the higher order term estimation. However, ray tracing simulations done for CHAMP reconstructed profiles show that for such profiles the correction formula (equation (21)) can correct about 80–85% Δs_3 error on an average.

6. Excess Path Length

[35] The difference in length between the curved path and the true range ρ is defined as the excess path length $d_I^{b(length)}$, and it can be written as

$$d_I^{b(length)} = \int_S^R ds - \rho \quad (22)$$

[36] It has been found that the excess path length depends not only on the TEC value but also on the ionosphere profile shape [*Jakowski et al.*, 1994]. In Figure 5, two ionosphere profiles (PROF 1 and PROF 2) are plotted, which have the same TEC value in vertical direction, but their shapes are different. At L2 frequency, the excess paths and TECs estimated by the ray tracing program using these two profiles are given in Table 1.

[37] Table 1 shows that, at L2 frequency and elevation 5°, the excess path lengths are about 27.5 mm for PROF 1 and about 7.6 mm for PROF 2. The corresponding TEC

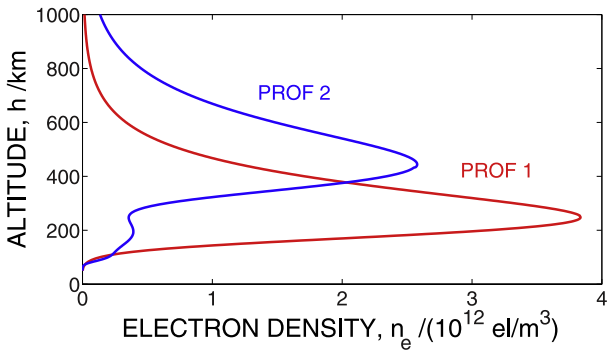

Figure 5. Ionosphere profiles with TEC_V = 100 TECU.

Table 1. Excess Path Length Error at L2 Frequency

	PROF 1		PROF 2	
Elevation (°)	TEC (TECU)	$d_I^{b(length)}$ (mm)	TEC (TECU)	$d_I^{b(length)}$ (mm)
1	335.7	37.46	263.84	9.56
5	322.07	27.51	257.05	7.57
10	289.62	17.12	239.59	5.38
30	174.93	2.92	163.16	1.33
60	113.34	0.26	111.77	0.12

along raypaths are estimated to be about 322.1 and 257.1 TECU, respectively. The excess paths per square TEC ($d_I^{b(length)}$/TEC^2) are estimated to be about 2.65×10^{-4} and 1.15×10^{-4} mm/TECU^2, respectively, for the two profiles at 5° elevation. The difference in $d_I^{b(length)}$/TEC^2 estimation indicates that the large variations in (slant) TEC measurement are not alone responsible for the large variations in the excess path length for the two profiles. The amount of curvature of the two profiles also influences the excess path length estimations. It has been found that the excess path is higher for a thin profile with large maximum ionization than for a thick profile with small maximum ionization.

[38] The ray tracing calculations have been carried out to compute $d_I^{b(length)}$ for a large number of geometrical and ionospheric conditions. Functional dependencies have been studied separately for each parameter to develop the empirical formula. Thus, the following formula has been obtained.

$$d_I^{b(length)} = \frac{7.5 \times 10^{-5} \cdot TEC^2 \cdot \exp(-2.13\beta)}{f^4 HF_2 \cdot (h_m F_2)^{1/8}} \qquad (23)$$

The excess path $d_I^{b(length)}$ will be measured in meters when TEC is in TEC units, frequency f in GHz, F_2 layer scale height HF_2 and peak ionization height h_mF_2 in kilometers, and elevation β is in radians. The dual-frequency residual error $\Delta s_{b(length)}$ can be estimated by equations (11) and (23).

[39] To check the accuracy of the correction formula (equation (23)), $\Delta s_{b(length)}$ is estimated for GPS L1–L2 signals in two ways: (1) by the ray tracing program using a large number of profiles (about 16200) and (2) by the correction formula (using equations (11) and (23)) knowing the TEC and the ionosphere parameters of F_2 layer of those profiles. The profiles are generated in such a way that TECs in vertical direction are same (in this case 100 TECU) for all profiles but their shapes will be different. The detail of this procedure is described in *Hoque and Jakowski* [2007]. The differences between excess paths estimated by the two methods are then calculated. These values are termed as remaining errors ($\Delta s_{b(length)}$ by first method $-\Delta s_{b(length)}$ by second method) and their statistical estimates such as root mean squared (RMS) error and maximum (MAX) error are given in Table 2 together with ray tracing results.

[40] We see that at 1° elevation, the RMS remaining error is less than 2 mm for the combined L1–L2 signal. The maximum error in the correction formula is found to be about 5.7 mm, whereas the maximum excess path can be as big as about 22.8 mm without correction (see Table 2). It has been found that on an average about 85% error will be corrected using the proposed correction formula (equations (23) and (11)). At high elevations (>60°), the excess paths are found to be small (<1 mm) at GPS frequencies and can be ignored.

[41] For CHAMP profiles, it has been found that the proposed correction formula (equations (23) and (11)) can correct about 70% $\Delta s_{b(length)}$ error on an average. The F_2 layer scale height HF_2 in the correction formula (equation (23)) is calculated by equation (19) knowing elevation, TEC, h_mF_2 and N_mF_2 values. The parameters h_mF_2 and N_mF_2 are known from the radio occultation data.

7. Range Error Due to TEC Difference at Two Frequencies

[42] As already mentioned, due to the dispersive nature of the ionosphere, two radio signals do not follow the same curved path. The traversed curved path through the ionosphere by a signal using Bouger's law of refraction can be written as [*Chen et al.*, 1990]

$$s = \int_{r_0}^{r} \frac{rn}{\sqrt{r^2n^2 - r_0^2 \cos^2 \beta_0}} dr \qquad (24)$$

where r_0 is the radial distance (from the Earth's center) of the receiver, β_0 is the elevation angle at the receiver, r and n are the radial distance and refractive index, respectively, at any point on the curved path, and dr is

Table 2. GPS Dual-Frequency (L1–L2) Residual Error $\Delta s_{b(length)}$

Elevation (°)	RMS Remaining Error (mm)	MAX Remaining Error (mm)	RMS $\Delta s_{b(length)}$ by Ray Tracing (mm)	MAX $\Delta s_{b(length)}$ by Ray Tracing (mm)
1	1.81	5.73	12.04	22.75
5	1.39	2.81	9.05	16.81
10	1.09	1.01	5.92	12.57
30	0.17	0.17	1.18	1.84
60	0.08	0.05	0.12	0.25

the raypath element. Equation (24) can be extended binomially as (detail is given in Appendix C)

$$s \approx \int_{r_0}^{r} \frac{r}{\sqrt{r^2 - a^2}} dr + \frac{Ka^2}{f^2} \int_{r_0}^{r} \frac{n_e r}{(r^2 - a^2)^{3/2}} dr + \frac{3K^2 a^2}{2f^4} \int_{r_0}^{r} \frac{n_e^2 r^3}{(r^2 - a^2)^{5/2}} dr \quad (25)$$

where $K = 40.3$ and $a = r_0 \cos \beta_0$. If the curved path is known, TEC can be estimated along that path multiplying it by the electron concentration n_e as

$$TEC_{path} \approx \int_{r_0}^{r} \frac{r n_e}{\sqrt{r^2 - a^2}} dr + \frac{Ka^2}{f^2} \int_{r_0}^{r} \frac{n_e^2 r}{(r^2 - a^2)^{3/2}} dr + \frac{3K^2 a^2}{2f^4} \int_{r_0}^{r} \frac{n_e^3 r^3}{(r^2 - a^2)^{5/2}} dr \quad (26)$$

We see that the first term on the right-hand side of equation (26) does not have frequency dependency. Therefore, for two different operating frequencies (e.g., f_1, f_2) this term will be equal and canceled out during difference method (see equation (8)). The third term is proportional to the inverse quartic power of frequency and its contribution to the TEC difference estimation is found to be negligible at L-band frequencies. Thus, the TEC difference can be estimated with sufficient accuracy by the second term of equation (26) at GNSS frequencies.

$$TEC_2 - TEC_1 \approx Ka^2 \left(\frac{1}{f_2^2} - \frac{1}{f_1^2} \right) \int_{r_0}^{r} \frac{n_e^2 r}{(r^2 - a^2)^{3/2}} dr \quad (27)$$

[43] Now to estimate the TEC difference by equation (27), we have to assume an ionosphere model for n_e. It has been found that L1 and L2 paths are largely separated (e.g., about 60 m at 7.5° elevation and TEC_V = 138 TECU [*Brunner and Gu*, 1991]) at and near peak electron density heights. Their separations on other parts through the ionosphere are not significant. As a result, the differences in TEC measurement along L1 and L2 paths mostly come from the ionosphere region at and near peak electron density heights.

[44] Therefore, it will be worthy looking for a function which can represent n_e at and near peak density heights very well and by which the integral equation (27) can be solved analytically. It has been found that a single quasi parabolic (QP) layer can be used for such a purpose.

[45] It should be mentioned here that the QP layer assumption is done only for deriving the TEC difference between two signal paths. The individual TEC measurement along L1 or L2 paths cannot be determined correctly in this approach. The vertical distribution of electron density given by a QP layer is [*Chen et al.*, 1990]

$$n_e(r) = \frac{A}{r^2} + \frac{B}{r} + C \quad (28)$$

in which $A = -(N_m \cdot r_m^2 \cdot r_b^2) / y_m^2$, $B = 2N_m \cdot r_m \cdot r_b^2 / y_m^2$, and $C = N_m - N_m \cdot r_b^2 / y_m^2$. The QP layer is only valid for $r_b < r < r_t$ where $r_b = r_m - y_m$, $r_t = r_m r_b / (r_b - y_m)$, r is the radial distance from the Earth's centre, r_m is the radial distance from the Earth's centre to the height of maximum ionization, N_m is the value of maximum ionization, and y_m is the layer semithickness.

[46] Now equation (27) can be solved analytically using the above n_e expression (equation (28)). The solution has been derived as

$$TEC_2 - TEC_1 = I_1 + I_2 + I_3 + I_4 + I_5 \quad (29)$$

in which

$$I_1 = \frac{KA^2 K_1}{a^3} \left[-\frac{a}{\sqrt{r^2 - a^2}} - \frac{3}{2} \cos^{-1} \left(\frac{a}{r} \right) - \frac{a\sqrt{r^2 - a^2}}{2r^2} \right]_{r_b}^{r_t}$$

$$I_2 = -\frac{2KABK_1}{a^2} \left(\frac{2r^2 - a^2}{r\sqrt{r^2 - a^2}} \right)_{r_b}^{r_t}$$

$$I_3 = -\frac{K(2AC + B^2)K_1}{a} \left[\frac{a}{\sqrt{r^2 - a^2}} + \cos^{-1} \left(\frac{a}{r} \right) \right]_{r_b}^{r_t}$$

$$I_4 = -2KBCK_1 \left(\frac{r}{\sqrt{r^2 - a^2}} \right)_{r_b}^{r_t}$$

$$I_5 = -KC^2 a^2 K_1 \left(\frac{1}{\sqrt{r^2 - a^2}} \right)_{r_b}^{r_t}$$

$$K_1 = \left(\frac{1}{f_2^2} - \frac{1}{f_1^2} \right) \quad (30)$$

Therefore, if the ionosphere parameters r_m, N_m, and y_m are known, the TEC difference can be estimated by equations (29) and (30). Thus, knowing the TEC difference, the residual error $\Delta s_{b(TEC)}$ can be determined by equation (8).

[47] From studies of ionospheric electron distribution [e.g., *Rishbeth and Garriott*, 1969; *Davies*, 1990], it is known that the QP layer can describe n_e well at and near peak electron density height; but it cannot describe n_e well at other heights. Although a Chapman layer can describe n_e along height very well, the equation (27) cannot be solved analytically using a Chapman layer. For this, a single QP layer representation of n_e is sought here.

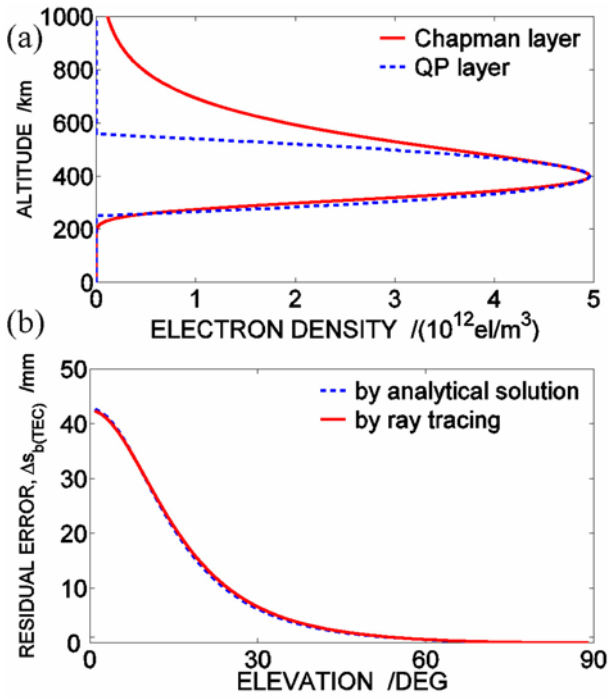

Figure 6. (a) A Chapman layer with H = 70 km and $N_m = 4.96 \times 10^{12}$ electrons/m^3 and a QP layer with y_m = 155 km and $N_m = 4.96 \times 10^{12}$ electrons/m^3, and (b) variations of $\Delta s_{b(\mathrm{TEC})}$ with elevation angle computed by the analytical solution (equations (8), (29), and (30)) and by the ray tracing program.

[48] Now the parameters describing the QP layer will have to be determined carefully. It has been seen that, at the peak electron density height, the curvature of a Chapman layer with scale height H is about the same as that at the apex of a parabola of semithickness $y_m = 2H$ [*Budden*, 1985]. However, it has been found that, for the assumption $y_m = 2H + 15$ (measured in km), the TEC differences (between L1 and L2 paths) estimated by the analytical integration method using a single layer QP function (equations (29) and (30)) have better convergence with those estimated by the ray tracing program using a Chapman layer. The maximum ionization and its height are considered to be same for both layers. Figure 6(a) shows a Chapman layer and the corresponding QP layer assumption. The residual error $\Delta s_{b(TEC)}$ is estimated by the analytical integration method using the QP layer and by the ray tracing program using the Chapman layer. These values are plotted in Figure 6(b).

[49] It has been found that at low elevation angles, $\Delta s_{b(TEC)}$ can be as big as about 4 cm during typical high ionosphere conditions ($\mathrm{TEC_V}$ = 143 TECU). The differences between $\Delta s_{b(TEC)}$ estimated by two methods are found to be less than 1 mm.

[50] However, the analytical solution for determining TEC difference is based on a single Chapman layer. But the actual ionosphere cannot always be described by a single Chapman layer; rather a number of layers are needed for this. Considering this, based on extended simulation studies using a large variety of ionosphere profiles, another correction formula has been developed to determine the excess TEC in addition to the LoS TEC at a given frequency.

$$\Delta TEC_i = \frac{0.1108 \cdot TEC^2 \cdot \exp(-2.1844\beta)}{f_i^2 HF_2 \cdot (h_m F_2)^{0.3}} \qquad (31)$$

where ΔTEC_i will be measured in electrons/m^2 when F_2 layer scale height HF_2 and peak ionization height h_mF_2 are in kilometers, frequency f_i is in Hertz, (slant) TEC is in electrons/m^2, and elevation β is in radians. Now, the residual error $\Delta s_{b(TEC)}$ can be estimated in meter by equation (8) in conjunction with equation (31).

[51] The residual error $\Delta s_{b(TEC)}$ is estimated by the ray tracing program and by the correction formula (equations (8) and (31)) for a large number of ionosphere profiles (about 3600) having the same $\mathrm{TEC_V}$ = 100 TECU. Then their differences ($\Delta s_{b(TEC)}$ by ray tracing $-\Delta s_{b(TEC)}$ by correction formula) are estimated and defined as remaining errors. The RMS and maximum (MAX) value of remaining errors are determined and given in Table 3 together with ray tracing results for selected elevation angles.

[52] We have found that, at 1° elevation angle and $\mathrm{TEC_V}$ = 100 TECU, the ray tracing $\Delta s_{b(\mathrm{TEC})}$ varies from 12 to 46 mm; this large variation in $\Delta s_{b(TEC)}$ is due to the variation in profile shapes. At 5° elevation angle, the RMS and maximum remaining errors are estimated to be about 3 and 10 mm, respectively. The corresponding RMS and maximum value in the ray tracing results are estimated to be about 22 and 40 mm, respectively.

[53] It has been found that, although the ionosphere profiles are modeled by four layers with wide range of layer parameters [given in *Hoque and Jakowski*, 2007],

Table 3. Statistical Estimates of $\Delta s_{b(TEC)}$

Elevation (°)	RMS of Remaining Error (mm)	MAX of Remaining Error (mm)	RMS $\Delta s_{b(TEC)}$ by Ray Tracing (mm)	MAX $\Delta s_{b(TEC)}$ by Ray Tracing (mm)
1	3.32	8.52	25.19	46.07
5	2.93	9.89	22.27	39.82
10	2.33	7.20	16.15	27.38
15	1.47	4.24	10.68	17.05
30	0.24	0.72	2.91	4.14
60	0.12	0.18	0.26	0.36

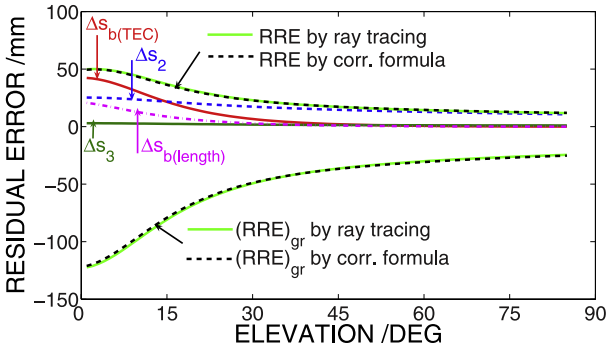

Figure 7. Comparisons of different higher order ionospheric errors when ionosphere is modelled by a Chapman layer with TEC_V = 143 TECU (Figure 6(a)).

the knowledge about the F_2 layer scale height and peak density height alone can eliminate about 85% error on an average.

[54] However, in practical cases, the information about F_2 layer scale height HF_2 and peak density height h_mF_2 are not easy to estimate. It has been found that using assumptions for HF_2 and h_mF_2, a significant amount of error can be corrected. For HF_2 = 70 km and h_mF_2 = 350 km, about 80% error will be removed on an average. Further investigation using CHAMP profiles shows that about 65% error will be corrected on an average by the correction formula.

8. Comparisons of Higher Order Ionospheric Errors

[55] Different higher order ionospheric errors are plotted in Figure 7. The residual error terms $\Delta s_{b(TEC)}$, Δs_2, Δs_3, and $\Delta s_{b(length)}$ are estimated by the ray tracing program while RRE and $(RRE)_{gr}$ are estimated by both the ray tracing program and by the correction formulas given in this paper. The correction formula for Δs_2 is given in *Hoque and Jakowski* [2007], and Δs_2 is estimated for azimuth angle 180° at a receiver position at (48°N and 15°E).

[56] Figure 7 shows that at low elevation angles (about <15°), the error component $\Delta s_{b(TEC)}$ is the highest among other errors and it decreases very rapidly with the increase of the elevation angle. It has been seen that at low elevation angles, Δs_2 is less than $\Delta s_{b(TEC)}$ but exceeds $\Delta s_{b(TEC)}$ with increasing elevation angle. The Δs_2 does not change significantly with increasing elevation angle and therefore, it cannot be ignored even at zenith. The third highest error is found to be the excess path length error $\Delta s_{b(length)}$. It decreases with increasing elevation angle very rapidly and vanishes at zenith. It has been seen that the residual error Δs_3 is small (∼<5 mm) but it can be bigger than $\Delta s_{b(TEC)}$ and $\Delta s_{b(length)}$ at high (about >60°) elevation angles.

[57] The excess path error $\Delta s_{b(length)}$ is additive to other errors in the $(RRE)_{gr}$ expression (see equation (6)) whereas it is subtractive in the RRE expression (see equation (7)). For this reason, $(RRE)_{gr}$ (absolute value) is much higher than RRE (see Figure 7). Figure 7 shows that RRE and $(RRE)_{gr}$ values estimated by the correction formulas converge with the ray tracing results. It has been found that for a Chapman profile the proposed correction formulas can estimate RRE and $(RRE)_{gr}$ within 1- to 2-mm level of accuracy.

9. Conclusions

[58] Although the second-order ionospheric term is considered in recent investigations, a common practice is to compute the magnetic field vector at the IPP assuming the ionosphere as a single layer at a certain altitude. Our investigation shows that computing average magnetic field component at the IPP introduces an additional error of about 0–2 mm in the GPS dual-frequency second-order error estimation.

[59] We have found that the dual-frequency third-order residual error can be as big as about 3 mm during high TEC values and low elevation angles such as TEC_V = 143 TECU and 1° elevation. The proposed third-order correction formula can correct this error within the submillimeter level of accuracy.

[60] The dual-frequency range error due to TEC difference at two GPS frequencies is found to be significant at low elevation angles (e.g., <15°). On the basis of analytical integration of raypath equation, an approximation formula has been derived to calculate TEC difference and consequent range error in dual-frequency measurements. It has been found that the analytical solution can correct this error within the 1-mm level of accuracy while the error without correction can exceed a 4-cm level for a Chapman layer with TEC_V = 143 TECU at elevation 1°. In addition, an empirical formula is developed for the same purpose.

[61] The excess path length of the signal in addition to the free space path length depends on ionosphere profile shapes. On the basis of simulation studies considering broader varieties of profile shapes, an approximation formula is developed to correct this error at GNSS frequencies. It has been found that, for the combined L1–L2 signal, the approximation formula corrects about 70–80% excess path length error on an average.

[62] In this paper, higher order ionospheric corrections are given for dual-frequency code and carrier-phase combinations. However, the noise on the code (the code noise may exceed 1 m whereas the phase noise is at the millimeter level [*Langley*, 1997; *Feng*, 2003]) may exceed the uncertainty in the higher order ionospheric

errors and make the corrections less attractive for code combinations.

[63] The availability of the third frequency from the modernized GPS and future Galileo systems and the interoperability of GPS and Galileo systems provide opportunities to eliminate higher order ionospheric effects by double and triple differencing methods which result in triple- and quadruple-frequency combinations, respectively. Using the triple-frequency approach, the second-order ionospheric error can be removed completely, but the range error due to TEC difference at three GPS/Galileo frequencies will not be canceled out completely. Future work is planned to investigate remaining errors in triple-frequency combinations.

Appendix A: TEC Approximation

[64] TEC along straight LoS can be written by the Chapman function as

$$TEC = N_0 \int_R^S e^{\frac{1}{2}(1-z-\sec\chi e^{-z})} dl \tag{A1}$$

where $z = (h - h_0)/H$, and dl is the differential increment in LoS direction (see Figure A1). Since the function inside the integral is in terms of $z(h)$, the element dl will be substituted by dz as follows. In the triangle ΔROS, we can write

$$(h + R_E)^2 = (R_h + R_E)^2 + l^2 - 2(R_h + R_E) l \cos(\beta + \pi/2) \tag{A2}$$

where R_h is the receiver altitude. Equation (A2) can be solved for l as

$$l = -(R_h + R_E)\sin\beta \pm \sqrt{(zH + h_0 + R_E)^2 - (R_h + R_E)^2 \cos^2\beta} \tag{A3}$$

where $Hz + h_0 = h$. Now equation (A3) will be differentiated and substituted in equation (A1)

$$dl = \pm \frac{H(zH + h_0 + R_E)}{\sqrt{(zH + h_0 + R_E)^2 - (R_h + R_E)^2 \cos^2\beta}} dz \tag{A4}$$

$$TEC = N_0 \int e^{\frac{1}{2}(1-z-\sec\chi e^{-z})} \frac{H(zH + b)}{\sqrt{(zH + b)^2 - a^2}} dz \tag{A5}$$

where $a = (R_h + R_E)\cos\beta$ and $b = h_0 + R_E$.
Substituting $x = zH + b$ and $Hdz = dx$ (using differentiation), equation (A5) becomes

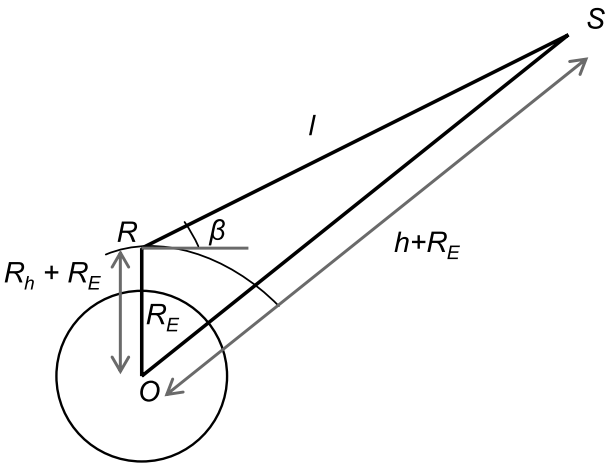

Figure A1. LoS raypath geometry where R, S, and O denote the receiver, satellite, and Earth's center positions, respectively, β is the elevation angle at the receiver, R_E is the radius of Earth, and l is LoS distance between R and S.

$$TEC = N_0\sqrt{e} \int e^{-\frac{x-b}{2H}} \cdot e^{-\frac{1}{2}\sec\chi \cdot e^{-\frac{x-b}{H}}} \frac{x}{\sqrt{x^2 - a^2}} dx \tag{A6}$$

If $a \ll x$ or $(R_h + R_E)\cos\beta \ll (R_h + R_E)$ (substituting x value at R_h), equation (A6) can be extended using binomial expansion. The assumption $a \ll x$ is valid at any elevation angle except $\beta = 0$. Under this assumption, equation (A6) can be expanded as

$$TEC = N_0\sqrt{e} \int e^{-\frac{x-b}{2H}} \cdot e^{-\frac{1}{2}\sec\chi \cdot e^{-\frac{x-b}{H}}} \cdot \left(1 + \frac{1}{2}\frac{a^2}{x^2} + \frac{3}{8}\frac{a^4}{x^4} + \frac{5}{16}\frac{a^6}{x^6} + \ldots\right) dx \tag{A7}$$

Now different terms of equation (A7) will be treated separately and added together to obtain the approximate solution for the slant TEC. The first term on the right-hand side of equation (A7) can be written after substituting $e^{-\frac{x-b}{2H}} = y$ and $e^{-\frac{x-b}{2H}} dx = -2Hdy$ (using differentiation) as

$$I_1 = -2HN_0\sqrt{e} \int e^{-\frac{1}{2}\sec\chi \cdot y^2} dy \tag{A8}$$

The second term on the right-hand side of equation (A7) can be written after substituting $e^{-\frac{x-b}{2H}} = y$, $x = b - 2H\ln y$ and $e^{-\frac{x-b}{2H}} dz = 2Hdy$ as

$$I_2 = -HN_0 a^2 \sqrt{e} \int \frac{e^{-\frac{1}{2}\sec\chi \cdot y^2}}{(b - 2H\ln y)^2} dy \tag{A9}$$

If $|2H\ln y| \ll |b|$ or $S_h - h_0 \ll h_0 + R_E$ (substituting $2H\ln y$ value at satellite height S_h), equation (A9) can be

extended using binomial expansion. This assumption is valid only when $S_h \ll (6371 + 2h_0)$ km. Under such assumption, equation (A9) becomes

$$I_2 = -\frac{HN_0a^2\sqrt{e}}{b^2}\int e^{-\frac{1}{2}\sec\chi\cdot y^2} \cdot\left[1+\frac{4H\ \ln y}{b}+\frac{3(2H\ \ln y)^2}{b^2}+\cdots\cdots\right]dy \quad \text{(A10)}$$

Similarly, the third term on the right-hand side of equation (A7) can be written as

$$I_3 = -\frac{3HN_0a^4\sqrt{e}}{4b^4}\int e^{-\frac{1}{2}\sec\chi\cdot y^2} \cdot\left[1+\frac{8H\ \ln y}{b}+\frac{10(2H\ \ln y)^2}{b^2}+\cdots\cdots\right]dy \quad \text{(A11)}$$

Now equation (A8) will be added to the first terms of equations (A10), (A11) . . ., as

$$I_{11} = \left(1+\frac{a^2}{2b^2}+\frac{3a^4}{8b^4}+\cdots\cdots\right) \cdot\left(-2HN_0\sqrt{e}\right)\int e^{-\frac{1}{2}\sec\chi\cdot y^2}dy = \left(1-\frac{a^2}{b^2}\right)^{-\frac{1}{2}}TEC_V = \frac{b}{\sqrt{b^2-a^2}}\cdot TEC_V \quad \text{(A12)}$$

where $\mathrm{TEC}_V = (-2HN_0\sqrt{e})\int e^{-\frac{1}{2}\sec\cdot y^2}\ dy$ and it can be approximated as [*Hoque and Jakowski*, 2007]

$$TEC_V = HN_0\sqrt{2e\pi\cos\chi} \quad \text{(A13)}$$

[65] Similarly, the second terms on the right-hand side of equations (A10) and (A11) can be added together to get I_{22}, but for simplicity we will ignore these terms here. Therefore, the TEC expression can be simplified combining equations (A12) and (A13) and substituting the values of a, b as

$$TEC \approx \frac{H(h_0+R_E)N_0\sqrt{2e\pi\cos\chi}}{\sqrt{(h_0+R_E)^2-(R_h+R_E)^2\cos^2\beta}} \quad \text{(A14)}$$

Appendix B: $\int n_e^2 dl$ Approximation

[66] Integrating n_e^2 along any direction (using Chapman function)

$$I = \int n_e^2 dl = N_0^2\int_{R_h}^{S_h} e^{(1-z-\sec\chi e^{-z})}dl \quad \text{(B1)}$$

Using the same procedure described in Appendix A for TEC approximation, equation (B1) can be manipulated and extended binomially as

$$I = eN_0^2\int e^{-\frac{x-b}{H}}\cdot e^{-\sec\chi e^{-\frac{x-b}{H}}} \cdot\left(1+\frac{1}{2}\frac{a^2}{x^2}+\frac{3}{8}\frac{a^4}{x^4}+\frac{5}{16}\frac{a^6}{x^6}+\ldots.\right)dx \quad \text{(B2)}$$

The first term on the right-hand side of equation (B2) can be written after substituting $y = e^{-\frac{x-b}{H}}$ and $-Hdy = e^{-\frac{x-b}{H}}dx$ as

$$I_1 = -eHN_0^2\int e^{-\sec\chi\cdot y}dy \quad \text{(B3)}$$

The second term on the right-hand side of equation (B2) can be written after substituting $e^{-\frac{x-b}{H}} = y$, $x = b - H\ln y$ and $e^{-\frac{x-b}{H}}dx = -Hdy$ as

$$I_2 = -\frac{eN_0^2Ha^2}{2}\int\frac{e^{-\sec\chi\cdot y}}{(b-H\ \ln y)^2}dy \quad \text{(B4)}$$

Now, equation (B4) can be extended as (see Appendix A)

$$I_2 = -\frac{eN_0^2Ha^2}{2b^2}\int e^{-\sec\chi\cdot y} \cdot\left[1+\frac{2H\ \ln y}{b}+\frac{3(H\ \ln y)^2}{b^2}+\cdots\cdots\right]dy \quad \text{(B5)}$$

Similarly, the third term on the right-hand side of equation (B2) can be extended as

$$I_3 = -\frac{3eN_0^2Ha^4}{8b^4}\int e^{-\sec\chi\cdot y} \cdot\left[1+\frac{4H\ \ln y}{b}+\frac{10(H\ \ln y)^2}{b^2}+\cdots\cdots\right]dy \quad \text{(B6)}$$

Now, equation (B3) will be added with the first terms of equations (B5), (B6),. . ., as

$$I_{11} = \left(-eHN_0^2\right)\left(1+\frac{a^2}{2b^2}+\frac{3a^4}{8b^4}+\cdots\cdots\right) \cdot\int e^{-\sec\chi\cdot y}dy = \left(-eHN_0^2\right)\left(1-\frac{a^2}{b^2}\right)^{-\frac{1}{2}}\left(\frac{e^{-\sec\chi\cdot y}}{-\sec\chi}\right) = \frac{beHN_0^2\cos\chi}{\sqrt{b^2-a^2}}\left(e^{-\sec\chi\cdot y}\right) \quad \text{(B7)}$$

Similarly, the second terms on the right-hand side of equations (B5), (B6),. . ., can be added together to get I_{22},

but for simplicity we will ignore these terms here. Therefore $\int n_e^2 dl$ expression can be simplified as

$$\int_{R_h}^{S_h} n_e^2 dl \approx \frac{beHN_0^2 \cos\chi}{\sqrt{b^2-a^2}} [e^{-\sec\chi \cdot y}]_{R_h}^{S_h} \quad \text{(B8)}$$

where $y = e^{-\frac{h-h_0}{H}}$. At $\chi = 0$ and for realistic H (range 60–80 km) and h_m (range 250–450 km) values, equation (B8) can be simplified as

$$\int n_e^2 dl \approx \frac{beHN_0^2}{\sqrt{b^2-a^2}} \approx \frac{H(h_m+R_E)N_m^2 \exp(1)}{\sqrt{(h_m+R_E)^2-(R_h+R_E)^2\cos^2\beta}} \quad \text{(B9)}$$

Appendix C: Curved Path Length Approximation

[67] If $r_0 \cos\beta_0 \ll rn$, equation (24) can be extended using binomial expansion. This assumption is valid except at very low elevation angle (i.e., $\beta_0 = 0°$). Under this assumption equation (24) can be written as

$$s = \int_{r_0}^{r} \left(1 + \frac{a^2}{2r^2n^2} + \frac{3a^4}{8r^4n^4} + \frac{5a^6}{16r^6n^6} + \ldots.\right) dr \quad \text{(C1)}$$

The index of refraction n (equation (14)) can be expanded in inverse powers of frequency [*Bassiri and Hajj*, 1993] as $n = 1 - 40.3 \cdot n_e/f^2$ (up to the second inverse powers of frequency). Using this assumption, the second term of equation (C1) can be extended using binomial expansion as

$$s_2 = \frac{a^2}{2}\int \frac{dr}{r^2n^2} = \frac{a^2}{2}\int \frac{1}{r^2}\left(1 + \frac{2Kn_e}{f^2} + \frac{3K^2n_e^2}{f^4} + \frac{4K^3n_e^3}{f^6} + \ldots.\right) dr \quad \text{(C2)}$$

where $K = 40.3$. Similarly, the third term of equation (C1) can be extended as

$$s_3 = \frac{3a^4}{8}\int \frac{dr}{r^4n^4} = \frac{3a^4}{8}\int \frac{1}{r^4} \cdot \left(1 + \frac{4Kn_e}{f^2} + \frac{10K^2n_e^2}{f^4} + \frac{20K^3n_e^3}{f^6} + \ldots.\right) dr \quad \text{(C3)}$$

Now the first term of equation (C1) will be added with the first terms of equations (C2), (C3),. . .

$$s_{11} = \int \left(1 + \frac{a^2}{2r^2} + \frac{3a^4}{8r^4} + \ldots...\right) dr = \int \left(1 - \frac{a^2}{r^2}\right)^{-1/2} dr = \int \frac{r}{\sqrt{r^2-a^2}} dr \quad \text{(C4)}$$

Adding the second terms on the right-hand side of equations (C2), (C3),. . ., we find

$$s_{22} = \int \left(\frac{a^2}{r^2}\frac{Kn_e}{f^2} + \frac{3a^4}{2r^4}\frac{Kn_e}{f^2} + \ldots...\right) dr = \frac{Ka^2}{f^2} \cdot \int \frac{n_e}{r^2}\left(1 - \frac{a^2}{r^2}\right)^{-3/2} dr = \frac{Ka^2}{f^2}\int \frac{n_e r}{(r^2-a^2)^{3/2}} dr \quad \text{(C5)}$$

Adding the third terms on the right-hand side of equations (C2), (C3),. . ., we find

$$s_{33} = \int \left(\frac{3a^2}{2r^2}\frac{K^2n_e^2}{f^4} + \frac{15a^4}{4r^4}\frac{K^2n_e^2}{f^4} + \ldots...\right) dr = \frac{3K^2a^2}{2f^4} \cdot \int \frac{n_e^2}{r^2}\left(1 - \frac{a^2}{r^2}\right)^{-5/2} dr = \frac{3K^2a^2}{2f^4}\int \frac{n_e^2 r^3}{(r^2-a^2)^{5/2}} dr \quad \text{(C6)}$$

Now the curved path length (equation (C1)) can be approximated adding all these expressions s_{11}, s_{22}, and s_{33}. The integral limit is also taken.

$$s \approx \int_{r_0}^{r} \frac{r}{\sqrt{r^2-a^2}} dr + \frac{Ka^2}{f^2}\int_{r_0}^{r} \frac{n_e r}{(r^2-a^2)^{3/2}} dr + \frac{3K^2a^2}{2f^4}\int_{r_0}^{r} \frac{n_e^2 r^3}{(r^2-a^2)^{5/2}} dr \quad \text{(C7)}$$

References

Bassiri, S., and G. A. Hajj (1993), Higher-order ionospheric effects on the global positioning system observables and means of modeling them, *Manuscr. Geod.*, *18*(6), 280–289.

Booker, H. G. (1949), Application of the magnetoionic theory to radio waves incident obliquely upon a horizontally stratified ionosphere, *J. Geophys. Res.*, *54*, 74–243.

Brunner, F. K., and M. Gu (1991), An improved model for the dual frequency ionospheric correction of GPS observations, *Manuscr. Geod.*, *16*(3), 205–214.

Budden, K. G. (Ed.) (1985), *The Propagation of Radio Waves: The Theory of Radio Waves of Low Power in the Ionosphere and Magnetosphere*, Cambridge Univ. Press, Cambridge.

Chen, J., P. L. Dyson, and J. A. Bennet (1990), Automatic fitting of Quasi-Parabolic segments to ionospheric profiles with application to ground range estimation for single-station location, *J. Atmos. Terr. Phys.*, *52*(4), 277.

Croft, T., and H. Hoogasian (1968), Exact ray calculations in a quasi-parabolic ionosphere with no magnetic field, *Radio Sci.*, *3*, 69.

Davies, K. (Ed.) (1990), *Ionospheric Radio*, Peter Peregrinus Ltd, London.

Feng, Y. (2003), Combined Galileo and GPS: A technical perspective, *J. Global Position. Syst.*, *2*(1), 67–72.

Fritsche, M., R. Dietrich, C. Knöfel, A. Rülke, S. Vey, M. Rothacher, and P. Steigenberger (2005), Impact of higher-order ionospheric terms on GPS estimates, *Geophys. Res. Lett.*, *32*, L23311, doi:10.1029/2005GL024342.

Hartmann, G. K., and R. Leitinger (1984), Range errors due to ionospheric and tropospheric effects for signal frequencies above 100 MHz, *Bull. Geod.*, *58*(2), 109–136.

Haselgrove, J. (1963), The Hamiltonian raypath equation, *J. Atmos. Terr. Phys.*, *25*, 397–399.

Hawarey, M., T. Hobiger, and H. Schuh (2005), Effects of the 2nd order ionospheric terms on VLBI measurements, *Geophys. Res. Lett.*, *32*, L11304, doi:10.1029/2005GL022729.

Hernandez-Pajares, M., J. M. Juan, J. Sanz, and R. Orus (2007), Second order ionospheric term in GPS: implementation and impact on geodetic estimates, *J. Geophys. Res.*, *112*, B08417, doi:10.1029/2006JB004707.

Hoque, M. M., and N. Jakowski (2006), Higher-order ionospheric effects in precise GNSS positioning, *J. Geod.*, *81*(4), 259–268, doi:10.1007/s00190-006-0106-0.

Hoque, M. M., and N. Jakowski (2007), Mitigation of higher order ionospheric effects on GNSS users in Europe, *GPS Solut.*, *12*(2), 87–97, doi:10.1007/s10291-007-0069-5.

Jakowski, N. (2005), Ionospheric GPS radio occultation measurements on board CHAMP, *GPS Solut.*, *9*, 88–95, doi:10.1007/s10291-005-0137-7.

Jakowski, N., F. Porsch, and G. Mayer (1994), Ionosphere-induced-ray-path bending effects in precise satellite positioning systems, *Z. Satell. Position. Navig. Kommun.*, *SPN 1/94*, 6–13.

Jakowski, N., A. Wehrenpfennig, S. Heise, Ch. Reigber, H. Lühr, L. Grunwaldt, and T. K. Meehan (2002), GPS radio occultation measurements of the ionosphere from CHAMP: Early results, *Geophys. Res. Lett.*, *29*(10), 1457, doi:10.1029/2001GL014364.

Kedar, S., G. Hajj, B. Wilson, and M. Heflin (2003), The effect of the second order GPS ionospheric correction on receiver positions, *Geophys. Res. Lett.*, *30*(16), 1829, doi:10.1029/2003GL017639.

Klobuchar, J. A. (1996), Ionospheric effects on GPS, in *Global Positioning System: Theory and Applications*, vol. I, edited by B. W. Parkinson and J. J. Spilker, pp. 485–515, American Institute of Aeronautics and Astronautics, Washington, DC.

Langley, R. B. (1997), The GPS error budget, *GPS World*, *8*(3), 51–56.

Leitinger, R., and E. Putz (1988), Ionospheric refraction errors and observables, in *Atmospheric Effects on the Geodetic Space Measurements*, edited by F. K. Brunner, *Monograph 12*, 81-102, School of Surveying, UNSW, Sydney.

Mandea, M., and S. Macmillan (2000), International Geomagnetic Reference Field—The eighth generation, *Earth Planets Space*, *52*(12), 1119–1124.

Nelder, J. A., and R. Mead (1965), A simplex method for function minimization, *Comput. J.*, *7*, 308–313.

Parkinson, B. W., and S. W. Gilbert (1983), NAVSTAR: Global Positioning System—Ten years later, *Proc. IEEE*, *71*, 1177–1186.

Rishbeth, H., and O. K. Garriott (Eds.) (1969), *Introduction to Ionospheric Physics*, Acad. Press, New York.

Strangeways, H. J. (2000), Nelder–Mead optimisation for ionopsheric HF path determination, *J. Atmos. Sol. Terr. Phys.*, *62*, 1361–1376.

Strangeways, H. J., and R. T. Ioannides (2002), Rigorous calculation of ionospheric effects on GPS Earth–satellite paths using a precise path determination methods, *Acta Geod. Geophys. Hung.*, *37*(2–3), 281–292.

M. M. Hoque and N. Jakowski, German Aerospace Center (DLR), Institute of Communications and Navigation, Kalkhorstweg 53, D-17235 Neustrelitz, Germany. (mainul.hoque@dlr.de; norbert.jakowski@dlr.de)